DEVELOPMENT OF A 1-CAMERA DOPPLER GLOBAL VELOCIMETER
- FIRST MEASUREMENT IN AN ROUND FREE JET -

Juliane A.C. Berthiau, Sebastien Goguey, Xavier Ottavy
Laboratoire de Mécanique des Fluides et d'Acoustique (LMFA),
UMR CNRS 5509,
École Centrale de Lyon, Université Claude Bernard Lyon 1, INSA Lyon,
69134 Ecully cedex, France

ABSTRACT

Doppler global velocimetry (DGV) has already been demonstrated as an interesting technique capable of measuring the three components of velocity in a plane. A 1-component DGV system is currently under development at Laboratoire de Mécanique des Fluides et d'Acoustique (LMFA), using a stabilized continuous wave (CW) Argon ion laser for emission. The receiver features only one camera for both *signal* and *reference* images and incorporate a *DEFI* system to adjust the incident laser light frequency and its transmission coefficient on the iodine cell absorption line. Optics have been chosen to reduce distortion and improve image contrast. Computer programs have been developed to help in the study of the iodine cell transmission profile, in the alignment process and eventually in images acquisition and processing to get velocity maps. Description of the whole system and first measurements in a round free jet are presented.

INTRODUCTION

Doppler global velocimetry (DGV) also called planar Doppler velocimetry (PDV) [1][2][3] or in some cases referred as filtered Rayleigh scattering velocimetry (FRS velocimetry) [4][5] is born in the 90's, almost simultaneously described by Komine et al. [6][7] and Miles et al. [8]. Since then, a few research groups have been refining this work, but the principles are unchanged. Based on the Doppler effect principle, DGV uses a laser light sheet to illuminate particles seeded in the gas flow. As those particles pass through the illuminated plane, they scatter light in all directions and the frequency of scattered light is shifted from the frequency of the incident light as shown on Fig. 1. The resulting Doppler shift $\Delta \nu$ is directly linked to the velocity vector $\vec{V}$ of the moving particles through the Doppler equation:

$$\Delta \nu = \nu - \nu_0 = \frac{1}{\lambda_0} \vec{V} \cdot \left(\vec{R} - \vec{E} \right) = \frac{V_p}{\lambda_0} \qquad (1)$$

where ν is the frequency of the scattered light, ν_0 the frequency of the incident light, λ_0 the incident light wavelength, $\vec{R}$ the observation direction and $\vec{E}$ the incident direction. The velocity component V_p which is a projection on the direction $(\vec{R} - \vec{E})$ indicates that one could determine the three components of the velocity vector by using either three observation directions or three illumination directions (or a combination of the two).

The major concept of DGV lies in the use of an absorption line of molecular species such as iodine vapour as a frequency-to-intensity converter. The laser frequency ν_0 is set to mid-point along one side of the absorption line so that any frequency shift is related to a change in light intensity. A camera can then be used to map the Doppler shift, and thus the velocity component, in grey levels of intensity.

Usually, the laser sheet is imaged by two cameras: one, termed the *reference* camera, views the laser sheet directly through the optics, and the other, the *signal* camera, views it through the absorption line filter (i.e. the frequency-to-intensity converter, using a iodine cell). The cameras are aligned and both images are calibrated so that they have the same scale and see the same zone on a pixel-to-pixel basis. By dividing the *signal* and the *reference* intensities at corresponding pixels, a transmission coefficient is calculated and used to obtain the Doppler shift. The velocity component for each pixel is eventually derived from equation (1). A crucial point with DGV is that each pixel corresponds to a specific measurement point and therefore, is illuminated and seen with its own specific directions. For this reason, the processing of the images should take into account those differences in the calculation of the velocity component.

As mentioned before, DGV has been refined by many research groups: a MHz-rate DGV system has been developed [9], a two-frequency DGV system [10][11], a combined technique named PPIDV [12] (planar particle

imaging Doppler velocimetry). But still, no commercial DGV system is available. The turbomachinery Team of LMFA at École Centrale de Lyon is currently developing its own system with the view of applying it for measurements in turbomachines. The aim of this paper is to discuss the different options and to comment our choices in the development of our DGV system.

EXPERIMENTAL SETUP OVERVIEW

The DGV measurement device developed at LMFA features two parts: the laser light sheet illumination set-up and the receiver set-up. Fig. 2 and Fig. 3 give an overview of the whole set-up (emission and reception parts respectively). To reduce costs and avoid synchronization problems, our receiver uses only one camera, like Chan's [13] or Ainsworth's [14]. It is based on the Mach-Zehnder interferometer design except that the second beamsplitter, which works as a combiner, is shifted so that the *reference* and the *signal* images are formed, side by side, on the CCD sensor. Details about each element of this DGV system will be discuss here-after in the paper.
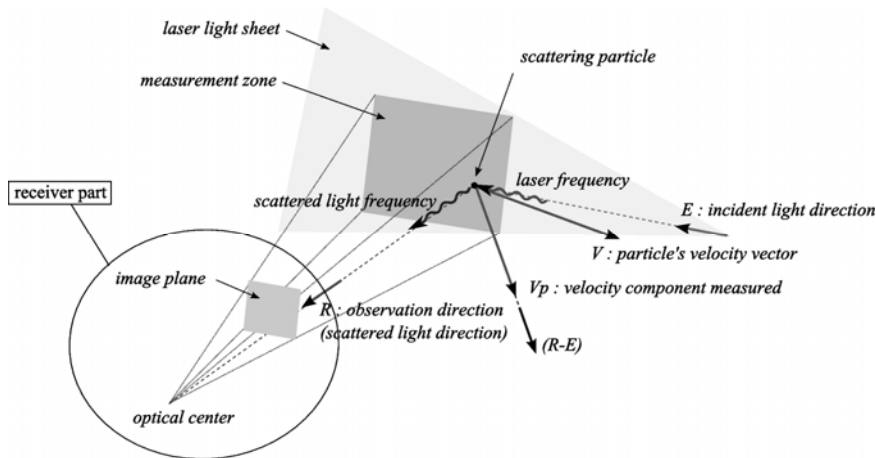
Fig. 1: DGV principle for measuring the component V_p on (R - E) of the particle's velocity vector V.
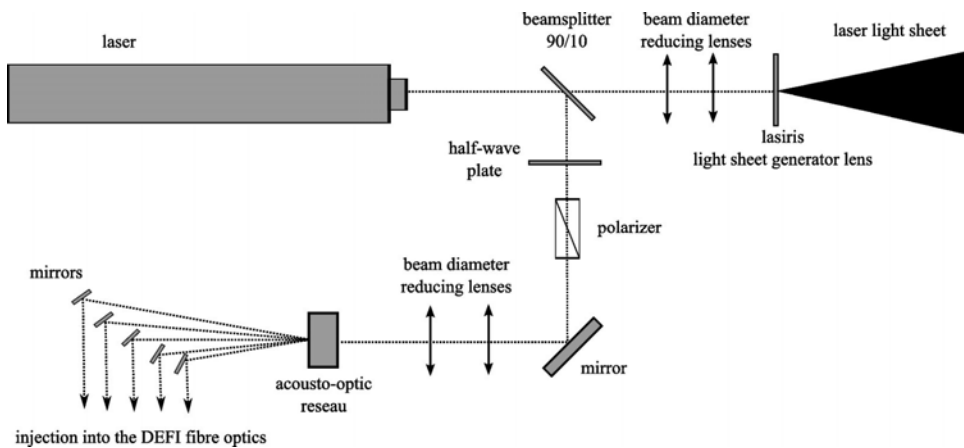
Fig. 2: Optical setup of the emission part of the DGV system.
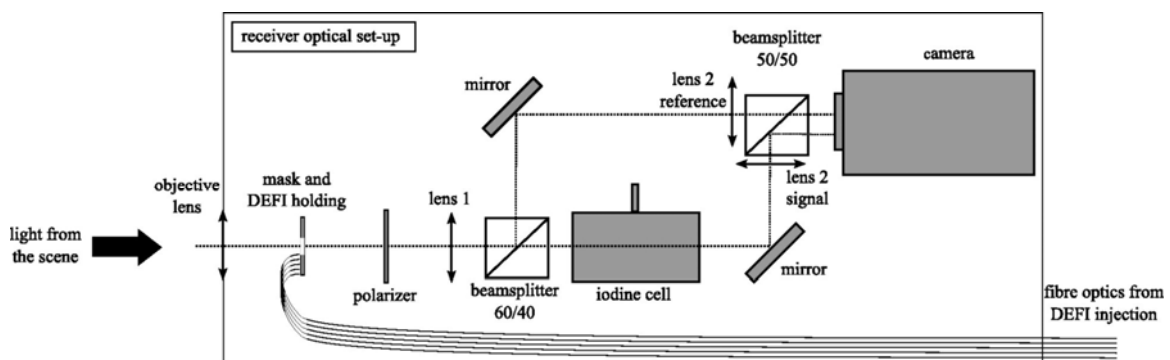
Fig. 3: Optical setup of the reception part of the DGV system.

LASER SOURCE AND ABSORPTION MEDIUM

Laser source

As with Mie scattering techniques, the first step in the process of building a DGV system is to choose the combination laser/absorbing medium. Most DGV system are using a molecular iodine I_2 vapour cell combined with either a continuous wave (*CW*) Argon ion laser at 514:5 nm or an injection seeded frequency doubled *Nd:YAG* pulsed laser at 532 nm. However, as suggested by Komine in his patent [6], molecular iodine is not the only possible choice: other species such as inter-halogen molecules, molecular bromine or alkali metals (caesium, rubidium, potassium, sodium and lithium) could provide absorption lines accessible by tuneable lasers like *CW* dye lasers [13][15].

Pulsed lasers enable high power laser sheet and instantaneous velocity field measurement, unfortunately, they require a device to monitor the laser frequency as it could considerably change between each pulse of about 100 MHz together with a frequency chirp (frequency variations across the laser beam) of about 100 MHz. Even if Elliott and Beutner mentioned in their review [16] that this could be reduced to 4 MHz by using only the central part of the beam, the use of pulsed lasers for DGV applications remains very complicated.

On the other hand, *CW* lasers have lower power but are quite easy to stabilize with a temperature controlled Fabry-Pérot interferometer in their cavity. It is therefore possible to operate continuously in single axial lasing mode with a very narrow bandwidth and fast frequency variations (jitter) reduced.

Since complete commercial solutions exist for *CW* laser, a *Spectra-Physics CW* Argon-ion laser model *BeamLok™ 2060* has been chosen. Thanks to a prism placed in the cavity, oscillation is limited to the 514:5 nm line. *Z-Lok™* (the above mentioned temperature stabilized etalon) and *J-Lok™* (a confocal interferometer providing feedback to the *Z-Lok™* etalon to stabilize the cavity length) systems allow for single frequency operation and reduced jitter: in power mode (i.e. operating for constant power output), one can achieve stabilized 2:0 W power in single longitudinal and transverse mode at full aperture with a linewidth of approximatively 10 MHz and jitter less than 2 MHz. Specifications report a frequency drift lower than 50 MHz/±C.

Iodine cell

Yeh and Cummins [17] were the first to determine the Doppler shift from light scattered by macromolecules using an heterodyne technique. In 1971, Devlin et al. [18] used an I_2 absorption cell to filter the undesired unshifted light in Rayleigh scattering applications. Shimizu [19] proposed in 1983 the use of an I_2 molecular filter as a narrowband, easy-to-use (compared to Fabry-Pérot interferometer) blocking filter for *LIDAR* application. Since then, atomic/molecular filters have now become of common use for laser stabilization, background suppression as well as *FRS* applications [13][4].

The numerous sharp absorption lines of iodine have been very much studied. The works of Tellinghuisen [20] can especially be cited here for his study of iodine atomic transitions. Gerstenkorn and Luc [21] looked at its absorption spectrum. Forkey [22] developed a theoretical model to predict the absorption profile, which works well to predict the position, the shape and the slope of the different iodine lines, but unfortunately over-estimate the maximum transmission coefficient and under-estimate the maximum absorption coefficient [23]. A key is to understand the absorption mechanisms that yield the frequency-to-intensity profile of the filter, with the objective of getting a stable sharp profile with the higher maximum and lower minimum transmission coefficients in order to maximize the sensitivity.

The absorption lines used with *CW* Argon ion lasers at 514:5 nm are around 19736 cm^{-1} (around 18788 cm^{-1} for *Nd:YAG* lasers). The absorption profile is not a constant, it depends from several parameters: the cell length of course since the amount of light absorbed depends of the number of molecules it encounters, the partial pressure (or number density) of the iodine vapour cloud, and its temperature. The width of the profile is mainly due to three mechanisms [16]: natural Lorentzian broadening caused by the finite time during which the atom is at the excited energy level yielding to the fact that the same excited state will have slightly different energy level for different atoms, collisional (or pressure) broadening caused by the atoms colliding with other chemical species (also referred as Lorentz, Holtsmark or Stark broadening, depending on the type of these species), thermal Doppler broadening caused by the thermal motion of the molecules absorbing light. Natural width is about 1 MHz, pressure broadening about 10 MHz and thermal broadening is of the order of 100 MHz. Moreover, the line is in fact the superimposition of many hyperfine lines broadened together (this explains the dissymetrical shape of the lines).

Different kinds of cell designs have been used and a detailed discussion on this subject is made by Chan et al. [13]. They advise using purest (i.e. highest grade) iodine 127 isotope and insist on the importance of avoiding any contamination during the degassing and filling process (see also [24] on this subject). Moreover they advise using a starved (also called superheated) type of cell instead of a simpler saturated model. In both cases, the cell is basically a glass cylinder with a side arm (or cold finger) and flat optical windows at each end. At constant

temperature of the cell body, the iodine partial pressure is controlled by the temperature of the cold finger, which is always a bit lower in order to prevent condensation in the cell body.

With saturated design cell, the transmission profile is strongly dependant on the partial pressure of iodine, which, in turn, is strongly dependent on the cold finger temperature. Crafton et al. [25] reported errors of ±5–15 MHz in the measured frequency for variations of ±0:1 K in the cold finger temperature. This sensitivity can be lower if the temperature is high enough to avoid any crystalline iodine to be present in the cell body and the cold finger. In that case, the cell is working saturated and the temperature control can be less accurate.

On the other hand, starved cell incorporate a stopcock, placed between the cell body and the cold finger, that enables operating without any crystalline iodine present in the cell body, setting the partial pressure constant and making the cell only dependent on the iodine vapour temperature.

Our cell is of the saturated type. It has been defined by Buchet [26] and manufactured by the BIPM (Bureau International des Poids et Mesures). It is 32 mm in diameter and 60 mm long (see Fig. 4). Temperature of the iodine is controlled via the cell walls temperature. Both the cell and the cold finger are wrapped with heating polyimide tape and two type J (Iron-Constantan) thermocouples measure their wall temperature: for the cold finger, the thermocouple is stuck directly onto the glass wall whereas for the cell body it is placed inside the metallic outer cylinder that surrounds the cell. This last outer cylinder is placed in a thermally insulated box to limit temperature deviations. Two PID (Proportional, Integral, Derivative) controllers allow a control of both temperatures with a precision better than ±0.5 K.

The cell was tested to determine its best operating conditions. The temperature of the body has been set to the maximum admissible temperature for the insulating material, it leads to T_{cell} = 70°C. Logically, it has been confirmed that at constant cell temperature, the higher the cold finger temperature is (and so the iodine partial pressure), the higher is the absorption. Indeed, we observed a decrease in the minimum transmission coefficient in the line and also a smaller decrease in the maximum transmission coefficient, out of the line (in the plateau). The sharpest profile was achieved for T_{finger} = 70°C.

With these temperatures, transmission profiles of the iodine cell have been obtained using the whole DGV system. The receiver part of our system took some pictures of a spot light (with a frequency fixed by the laser source) on a black painted disk. Note that the disk had a very small rotating speed, just to average the effect of the surface non-uniformity. The light powers for the *reference* and the *signal* images have been calculated with our image processing software (see the *image processing* section). The transmission coefficients have been calculated using the ratio of the *signal* and the *reference* light powers, and normalized by the maximum transmission coefficient given by the plateau. Fig. 5 shows the absorption of the iodine cell changing discontinuously, according to the mode hops of the laser frequency. Only the right flank of the absorption line is presented and used, because its slope is steeper than the one of the left flank and, as a consequence leads to a better sensitivity of the system. The frequency on the X-axis has been arbitary set to 0 for the minimum transmission coefficient which is about 3.6%. The results of 16 cases are summarized on this figure and show very small discrepancies between each other. Those observations lead to the conclusions that, first our image processing is accurate and secondly that the cell must be operating saturated. This would indeed explain why only slight variations of the profile were observed as they were caused by very small changes in the global iodine cloud temperature.

In order to measure a velocity component, a continuous curve of the frequency shift as a function of the absorption transmission coefficient has to be established. This continuous iodine absorption profile is achieved with an interpolation using a Boltzmann derived function written as:

$$T = \frac{1-T_{\min}}{1+exp\left(\dfrac{\nu-\nu_{offset}}{a}\right)}+T_{\min} \qquad (2)$$

where T is the transmission coefficient, T_{min} the minimum transmission coefficient, ν the light frequency, ν_{offset} a horizontal frequency offset related to the arbitrary choice of having a null frequency at the start of the X-axis, and a a horizontal stretching constant. T_{min}, ν_{offset} and a are determined by the fit process. Moreover, because the bottom and the top part of the absorption iodine profile are not symmetrical, two fits have been calculated and summarized in table below. The resulting fit is plotted in Fig. 5, see continous curve.

with $\nu \leq 800$ MHz		with $\nu > 800$ MHz		
ν_{offset}	700.0 MHz	ν_{offset}	707.5 MHz	(3)
T_{min}	0.03459	T_{min}	0.03459	
a	-116	a	-107	
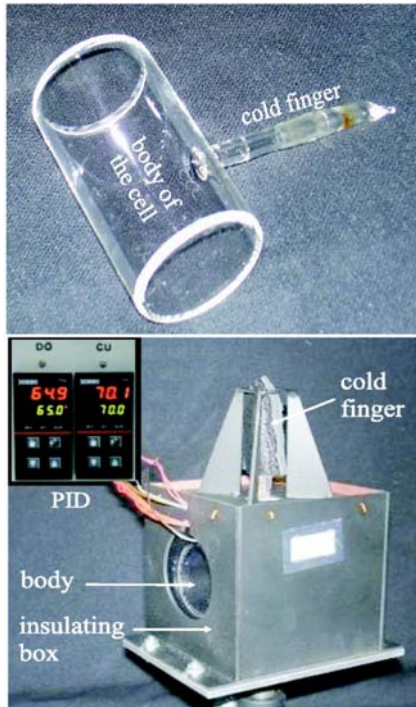
Fig. 4: Iodine cell (top) and Iodine cell in its insulated box with its PID controller (bottom).
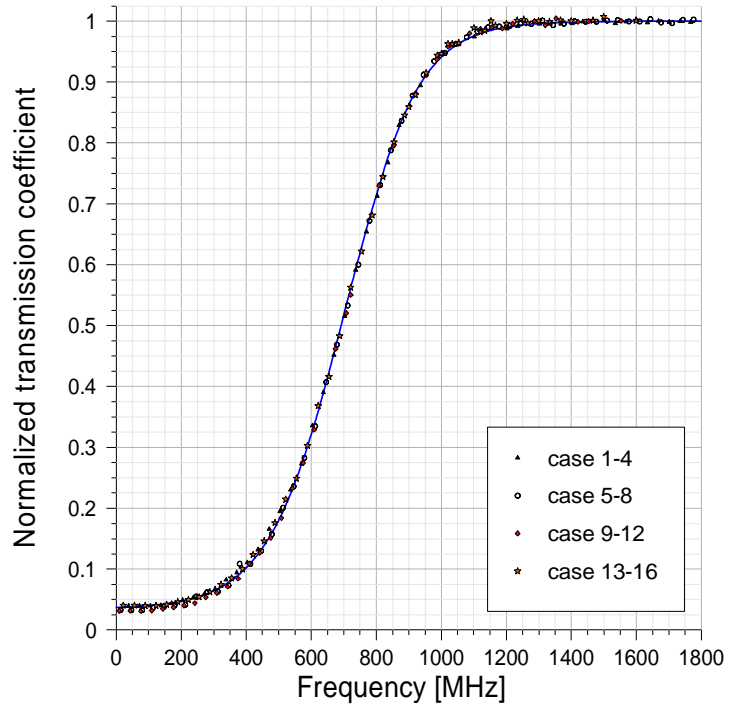
Fig. 5: Normalized transmission coefficient obtained in the right flank of Iodine cell absorption line.

OPTICS

Laser sheet generation

The laser light coming from the *CW* laser has a Gaussian light intensity distribution. In order to obtain a light plane with a constant intensity, a *Lasiris* lens from *Laser 2000* is used. With a 1.3 mm incident beam diameter, a sheet is generated with an opening angle of 5°; a variation of only 3% in the laser light sheet intensity is observed. As shown in the sketch of Fig. 2, a part of the emitted laser light is picked off for the *DEFI* system (see section "*2. Laser frequency and iodine profile monitoring system*" for details about this system). A half-wave plate combined with a polarizer is used as a variable attenuator in order to adjust the power at the entrance of the acousto-optic grating and avoid any saturation of the corresponding image pixels in the DGV images.

Camera

The CCD camera is a key component of the system. The main requirement for DGV camera is high digitizing as this represents the number of grey levels on which the intensity will be recorded. The *PCO Sensicam QE* frame transfer camera we chose has a 12-bit analog-to-digital converter (so a 500 MHz edge of the absorption line would be discretized in 4096 levels of 0.122 MHz each). The CCD is cooled by a 2-stage Peltier cooler with forced air cooling to keep it at -11°C ; readout noise is very low about 4 to 6 e⁻ *rms* depending on the gain. Exposure time is ranging from 500 ns to 1000 s. Besides, the fill factor is 99% which means the spatial discretization of the measurement zone is very good (no holes between the points). Finally, it responses well at the light frequency (quantum efficiency: 62 % at 500 nm), and the number of pixels (1376 * 1040) is sufficient for our application. Binning mode is also available, from 1 to 8 horizontally and from 1 to 32 vertically.

Receiver setup

Almost each team working on DGV has its own receiver set-up. Fig. 6 is a picture of the setup built from the sketch of Fig. 3. In such a configuration, the focusing length D_f and the depth of field PC, which have to be optimized for the DGV measurement, depend on many parameters: the three focal lengths f_0; f_1; f_2, the distance d_{12} between lens L_1 and lens L_2, the global magnification of the receiver G and the distance d between L_0 image plane and L_1 object plane. On top of those parameters, PC also depends on the aperture ratio number N of the objective lens L_0, and on the theoretical focusing tolerance which corresponds to the pixel size: 6.45 μm.
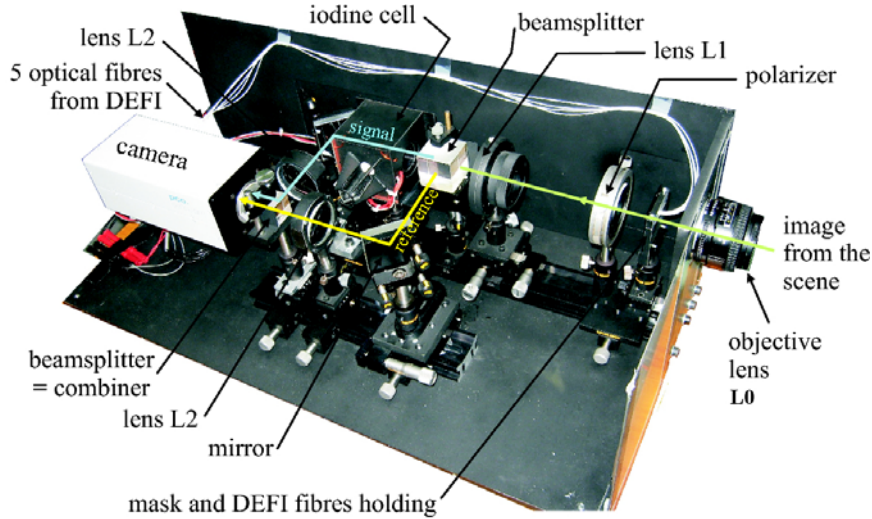
Fig. 6: Receiver setup.

To get the same magnification ratio G for both *reference* and *signal* optical images, even if they have not the same path length, it is a requirement to split L_1 and L_2 and to have a collimated beam between them, i.e. $d = 0$. Besides, the five *DEFI* light spots and the mask that is used as a matte must be in the focal object plane of L_1 to be focused. This also requires that the ratio f_2/f_1 to be adapted to the *DEFI* spots size and the CCD pixels size.

A model based on geometric optics has been developed to study those dependencies. It has been used to determine a configuration that enables both assembly and measurement. Eventually, achromatic doublets of focal lengths $f_1 = 160$ mm and $f_2 = 80$ mm are used. They are spaced by $d_{12} = 250$ mm where the beamsplitter, the iodine cell and the signal mirror can lie. For a magnification ratio $G = 0.03$, corresponding to a measurement zone with size of about $80*200$ mm^2, two objective lenses L_0 are available and can be used, leading to two configurations:

f_0	N	D_f	PC
28 mm	5.6	495 mm	42 mm
50 mm	8	883 mm	61 mm

where D_f and PC have been calculated from our model. The relation for D_f is expressed here after. The one for PC is a bit complicated and have no interest to be presented in this paper.

$$D_f = f_0 \cdot \left(1 + \frac{f_1 \cdot f_2}{d \cdot G \cdot \left(f_2 - d_{12} + \frac{f_1 \cdot (d + f_1)}{d} \right)} \right) \tag{4}$$

Changing the objective lens L_0 enables changing D_f and PC if working at constant G, or changing G if working at constant D_f. Those results show small depth of fields but this is to link to the focusing tolerance that has been chosen very small. Practically these depth of fields are in fact high enough for measurement. Increasing N would increase PC but also distortions and coma aberrations. On the other hand, decreasing it would increase spherical aberrations (and so decrease image contrast) and increase the collimated beam diameter above the iodine cell diameter.

Cube beamsplitters were preferred to plate as they avoid distortions. However, because their transmission coefficients follow Fresnel's equations for reflection, optics must be designed to deal with any polarization variations (in the scattered light from the scene but also in light coming out of the optical fibres) or the ratio between *signal* and *reference* sub-images will not only be a function of the Doppler shift. This is done through a polarizer, placed just before lens L_1, which forced the polarisation directions to be the same for each points so that the transmission and reflection coefficients of the beamsplitters stay constant. The main disadvantage of this technique is that it highly decreases the intensity of the light coming from the scene.

Finally, care must be taken in the collimation process to ensure good contrast, low distortions and good focus on the CCD, proper alignment of the reference and signal sub-images, together with the same

magnification ratio. Because a diffraction halo caused by the mask was polluting the DEFI optical fibres zone at the top of both sub-images, a diaphragm was added just after L_1 where the image beam is collimated.

Alignment process

To ensure good alignment of the receiver optics, a test card (black dots regularly spaced on a white background) is placed in front of the objective lens, in the object plane. Our software detects the dots by means of a local threshold algorithm, and monitor continuously (to allow live correction) their relative position. Firstly rotation is checked. Secondly, the position of L_1 is adjusted to get the same magnification ratio on both sub-images and therefore a collimated beam between L_1 and L_2. Finally the position of the combiner beamsplitter is adjusted to get a sub-pixel matching between both sub-images on the CCD sensor. Note that thanks to the camera calibration (see next section) a sub-pixel matching is not necessary for DGV measurements.

DGV MEASUREMENT STEPS

The velocity measurement using our DGV system is achieved by following different steps in the right order. We therefore developed a modular computer software, based on the LabView™ language. The program helps, in the measurement process, to:

1. do the incident laser light direction calibration
2. perform the pixel-to-pixel calibration and observation direction calibration
3. position the laser frequency in and out of the iodine absorption line
4. acquire and process the images
5. deduce the Doppler frequency shift maps and calculate the velocity component.

1. Incident laser light direction calibration

Determination of the incident light direction $\vec{E}$ is obtained through analysis of the shades made by an object like a comb placed in the emitted laser light sheet, which has been seeded. An extrapolation is then done to get the coordinates of $\vec{E}$ for each point of the image.

2. Pixel-to-pixel and observation direction calibration

The aim of the pixel-to-pixel calibration is to link each pixels of the *reference* and *signal* sub-images to the corresponding measurement zone and to determine the observation direction $\vec{R}$ for each of them. To do this, the camera, placed at its measurements position, views the measurement plane where again a dot-card image is acquired. Detection and localization of each dots is then performed. Next, one must relate the coordinates of a point P_w in the object plane to the coordinates of the corresponding pixel P_d on the image, this is where camera models are needed.

In their very complete review, Salvi et al. [29] present different models for camera calibration and propose some unified notations. Fig. 7 shows the four usual steps of the calibration and those notations: left superscript defines the coordinate system (W for world, C for camera, R for retina, I for image), letter and right superscript describe the point. The first step consists in changing from the world coordinate system, in which the object point coordinates are expressed, to the camera coordinate system. Next, a projective transformation is applied to P_w and its projection P_u on the retina plane is determined. A distortion model is then applied to find the final distorted point P_d. A last change to the image coordinate system is eventually done.

The model we used is Tsaï camera model with radial distortion and full non-linear parameters optimization. The aim of the calibration is to determine the camera external and internal parameters. External parameters describe the position of the camera relative to the object plan: a rotation matrix and a translation vector. Internal parameters on the other hand, describe the optical properties of the whole receiver system: the focal distance F, the coordinates C_x and C_y of the centre O_r of the image, the skewness angle and the distortion parameters (that can be reduced to its first order parameter). One could refer to Salvi et al. [29] for a detailed description of the method to implement calibration. Also, literature on this subject is very wide: recently, Willert [30] and Zollner and Sablatnig [31] compared camera models for use in planar calibration: general pinhole model using direct linear transformation (*DLT*), Tsaï camera model without and with optimization, and Zhangs method that requires three calibration images. Besides both PhD theses of Toscani [32] and Bénallal [33] are of great interest to understand those models.

Once the external and internal parameters are known, it is possible to change directly from the pixel location on each sub-images to the corresponding measurement zone and thus to deduce the correspondence between each *reference* and *signal* pixels. Moreover, the observation direction vector $\vec{R}$ is directly given by a change into the camera coordinate system.
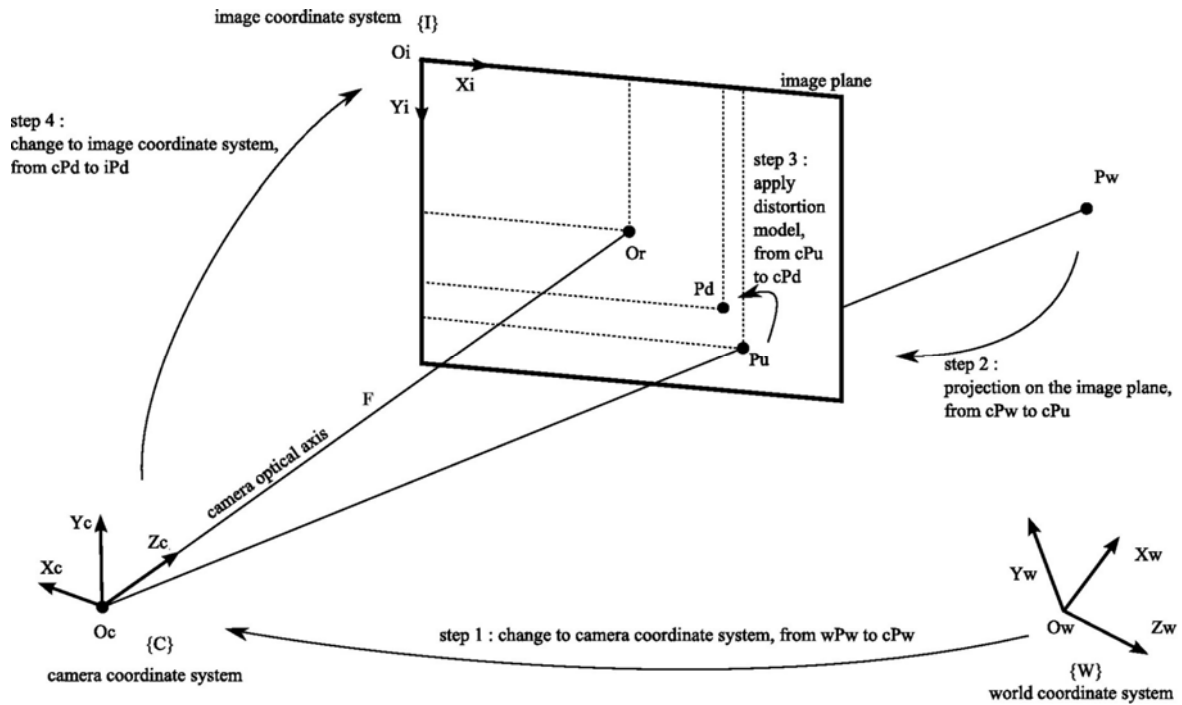
Fig. 7: Camera calibration principle.

3. Laser frequency and iodine profile monitoring system

Different techniques are used to monitor laser frequency drift and/or iodine transmission profile. One of the simpler approaches consists in imaging a stationary object to provide a not-shifted frequency reference [11]. Another common (but less easy) approach is to use a second iodine cell to monitor the laser frequency drift [24] [27]. The method chosen here is inspired by the one developed by ONERA [28] and patented with the name *DEFI*.

The principle is to extract a sample of the emitted laser beam, with its frequency ν_0, and send it through an acousto-optic grating, working in the Raman diffraction regime, in order to get five laser beams with 5 different frequencies: ν_0 - 200 MHz, ν_0 - 100 MHz, ν_0, ν_0 + 100 MHz and ν_0 + 200 MHz. Those five beams are then injected in five optical fibres whose exits are placed in the receiver (reception part of the DGV system), in an intermediate image plane, in front of the beamsplitter and the iodine cell (see Fig. 2 and Fig. 3). The top of each DGV images (*reference* and *signal*) is dedicated to the five *DEFI* light spots. Five transmission coefficients are so calculated in order to monitor the iodine transmission profile and deduce the position of the laser frequency directly from the DGV images.

This method is interesting to set the laser frequency in the iodine absorption line or on the maximum transmission plateau, depending on the image that has to be acquired, but it is not very accurate to determine the iodine absorption line profile with only five points. In our case, the transmission profile of the iodine cell is already accurately known, and it has shown very god repeatability when using the cell under the same conditions (i.e. with same temperatures for the body and the finger of the cell, see Fig. 5). The *DEFI* is just used to determine more accurately the frequency emitted by the laser source during the images acquisition. Five transmission coefficients are calculated from the five *DEFI* light spots and are fitted on the transmission profile with the method of least squares applied to relation (2) where the variable to be optimized is the frequency ν_0 and its 4 modes (ν_0 - 200 MHz, ν_0 - 100 MHz, ν_0 + 100 MHz and ν_0 + 200 MHz). This method has demonstrated a lot of benefits regarding the results obtained in the case of the velocity measurements of solid points on a rotating disk surface. These measurements are not presented in this paper.

4. Image processing

Firstly, two images are required to qualify the camera. Those images, which have been taken with the camera off the receiver system, enable the identification of defective pixels. A first image called I_{black} is therefore taken with the cap on the CCD sensor in order to identify hot pixels (i.e. pixels whose response are too high). A second image called I_{flat} is taken of an uniformly illuminated card placed just in front of the CCD sensor, in order to detect cold, or even dead, pixels (i.e. pixels whose response are too low). Defective pixels are then listed and will be removed from the DGV images.

Secondly, four images are necessary to perform the DGV measurement. The most important image is the DGV image I_{line}, achieved with the laser light sheet illuminating the flow seeded with the particles. The subscript *line* refers to the position of the laser frequency around the middle of the right flank of the absorption line. The second image is named $I_{plateau}$. It is taken with the same exposure time and seeding conditions as I_{line}, but with the position of the laser frequency on the plateau of the iodine absorption profile, i.e. the maximum transmission coefficient. The third and fourth images are the background images $I_{bkg-line}$ and $I_{bkg-plateau}$ which are respectively taken in exactly the same conditions (exposure time, gas flow, laser frequency) as I_{line} and $I_{plateau}$, except that the flow is not seeded with particles.

Those background images are subtracted to I_{line} and $I_{plateau}$ in order to remove the thermal and noise signals, so as to keep only the DGV signal. As they were taken without any seeded particle, no Doppler effect occurs. The resulting images I^{*}_{line} (= I_{line} - $I_{bkg-line}$) and $I^{*}_{plateau}$ (= $I_{plateau}$ - $I_{bkg-plateau}$) are then used to obtain a normalized image R. Indeed, pixels of the CCD sensor do not response identically: the number of hitting photons required to produce one electron is not the same for each pixel. This means that a uniform lightning will not necessarily result in a uniform image. For this reason $I_{plateau}$, which differs from I_{line} only by the fact that the laser frequency is set to a point where Doppler shift do not results in any change in the transmission coefficient, provides a good normalization image.

Note that a threshold, corresponding to a percentage of the maximum pixel intensity of I^{*}_{line} and $I^{*}_{plateau}$ images, is used to filter the pixels with very low noise to signal ratio. This is especially the case in the zones where the seeding is low, leading to a very low intensity of the scattered light.

Finally, the DGV image R is split into two sub-images called R_{ref} and R_{sig} respectively corresponding to the part of the image which followed the *reference* or *signal* optical path. Once R_{ref} and R_{sig} are obtained, the transmission coefficient is directly obtained by dividing them on a pixel-to-pixel basis.

In short, the processing follows those steps:

1. defective pixels detection on I_{black} and I_{flat}

2. background suppression: $I^{*}_{line} = I_{line} - I_{bkg-line}$ and $I^{*}_{plateau} = I_{plateau} - I_{bkg-plateau}$

3. correction for the non-uniform pixel response: $R = I^{*}_{line} / I^{*}_{plateau}$

4. R split between R_{ref} and R_{sig}.

5. removal of the defective pixels.

6. calculation of the transmission coefficient: $T = R_{sig} / R_{ref}$

5. Doppler frequency shift and velocity component maps

With the map of the transmission coefficient of each pixel, it is then straightforward to compute the Doppler shift using relation (5), which comes from equation (2) taking into account the frequency ν_0 of the laser light during the acquisition of the I_{line} image.

$$\Delta\nu = \nu - \nu_0 = a.ln\left(\frac{1-T}{T-T_{min}}\right) + \nu_{offset} - \nu_0 \tag{5}$$

With the knowledge of the incident light $\vec{E}$ and observation $\vec{R}$ vectors that have been determined by the calibrations, the velocity component V_p is finally obtained through equation (1).

MEASUREMENTS IN A ROUND FREE JET

The first measurements have been carried out in a round free jet. The laser light sheet that represents the plane where the measurements are done is perpendicular to the axe of the jet and is located at one diameter from the jet exit. This location means that part of the flow is in the potential cone of the jet with a constant velocity that will help to compare our results. Fig. 8 presents the geometrical configuration of these measurements, with locations and angles for the emission and reception part of the DGV system.

Both the *reference* and *signal* images result from an average of 64 shoots. After the data processing, the axial velocity is plotted in Fig. 9 for each pixels associated with the measurement zone. A threshold of 10% of the maximum light intensity for these two images has been used during the image processing. That explains why the velocity values drop suddenly to zero at the boundary of the jet, instead of reaching it asymptotically. These results show good agreements with classical pressure probe measurements for the maximum velocity in the potential zone.

A few remarks can be done after this test:

- The iodine absorption profile and the incident laser light frequency have to be known very accurately because they constitute the critical part of the uncertainties.

- The results presented in this paper are steady results (averaged). Instantaneous measurements are limited at the moment by the exposure time of the camera. Beside, we noticed that the laser frequency fluctuates in a range of about ±15 MHz around its mean value. This will be a serious problem to be solved before doing unsteady measurements with such DGV system.

- The tune of the laser is achieved by changing the temperature of the etalon in the Fabry-Pérot interferometer. Setting the laser frequency in the middle of the right flank of the iodine absorption line and in the plateau is time consuming.
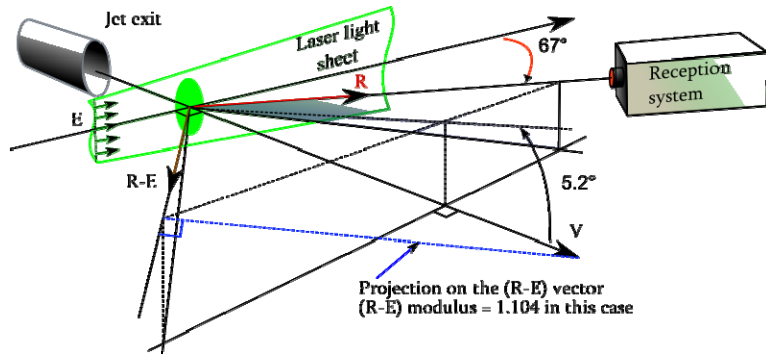
The zone of the DGV image that concerns the seeded area is defined with 172*182 pixels, corresponding to a square in the world frame of 30*30 mm².

Fig. 8: Geometric configuration for measurements in a round free jet – x/d = 1.0.
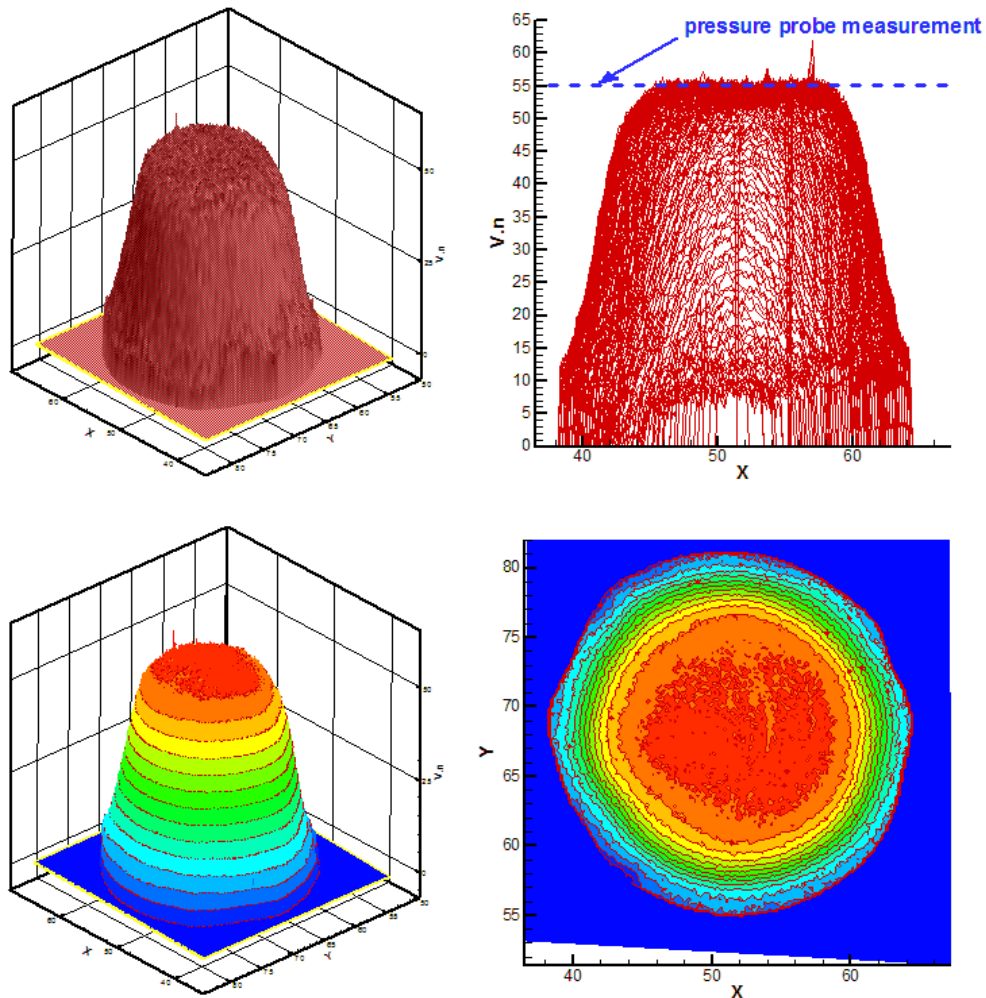
Fig. 9: Axial velocity distribution in a round free jet – x/d = 1.0.

CONCLUSION

A 1-component Doppler global velocimeter is under development at LMFA. The different elements of the measurement system have been studied, chosen and assembled. First measurements have been done on a rotating disk in order to avoid any troubles with seeding and aerodynamics. Results have demonstrated the importance of the accurate definition of the iodine absorption profile and of the correct determination of laser light frequency during the acquisition. The fluctuations of the laser frequency around its mean value and the time exposure needed by the camera to shoot the DGV images impose steady (averaged) results. 1D measurements for complete validation are carried out at the moment on round free jet. First measurements have revealed very good agreements in terms of mean value of the velocity compared to classical pressure probe measurements. Detailed characterization of the flow field in this round free jet will give crucial answers to know if the DGV system could be an interesting measurement technique for turbomachinery applications.

ACKNOWLEDGEMENTS

REFERENCES

[1] R.L. McKenzie. Measurement capabilities of planar Doppler velocimetry using pulsed lasers. Applied Optics, 35(6):948–964, February 1996. also in: 33rd AIAA Aerospace Sciences Meeting and Exhibit, Reno, Nevada, 9–12 January 1995, AIAA Paper 95-0297.

[2] P. Clancy and M. Samimy. Two-component planar Doppler velocimetry in high speed flows. AIAA Journal, 35(11):1729–1738, November 1997.

[3] A.D. Mosedale, G.S. Elliott, C.D. Carter, and T.J. Beutner. Planar Doppler velocimetry in a large-scale facility. AIAA Journal, 38(6):1010–1024, June 2000.

[4] M. Boguszko and G.S. Elliott. Property measurement utilizing atomic/molecular filter-based diagnostics. Progress in Aerospace Sciences, 41(2):93–142, February 2005.

[5] J.P.R. Gustavsson and C. Segal. Filtered Rayleigh scattering velocimetry – accuracy investigation in a M=2.2 axisymmetric jet. Experiments in Fluids, 38(1):11–20, January 2005.

[6] H. Komine. System for measuring velocity field of fluid flow utilizing a laser-doppler spectral image converter. United States Patent 4919536, April 24, 1990.

[7] H. Komine, S.J. Brosnan, A.B. Litton, and E.A. Stappaerts. Real-time Doppler global velocimetry. In 29th AIAA Aerospace Sciences Meeting, Reno, Nevada, US, January 7–10, 1991. AIAA Paper 91-0337.

[8] R.B. Miles, W.R. Lempert, and J.N. Forkey. Instantaneous velocity fields and background suppression by filtered Rayleigh scattering. In 29th AIAA Aerospace Sciences Meeting, Reno, Nevada, US, January 7–10, 1991. AIAA Paper 91-0357.

[9] B. Thurow, N. Jiang, W.R. Lempert, and M. Samimy. MHz rate planar Doppler velocimetry in supersonic jets. In 42nd AIAA Aerospace Sciences Meeting and Exhibit, Reno, Nevada, US, January 5–8, 2004. AIAA Paper 2004-0023.

[10] S.A. Arnette, G.S. Elliott, A.D. Mosedale, and C.D. Carter. Two-color planar Doppler velocimetry. AIAA Journal, 38(11):2001–2006, November 2000.

[11] T.O.H. Charrett. Development of two-frequency Planar Doppler Velocimetry instrumentation. PhD thesis, Cranfield University, Cranfield University, Cranfield, UK, 2006.

[12] M.P.Wernet. Planar particle imaging Doppler velocimetry: a three component velocity measurement technique. AIAA Journal, 43(3):479–488, March 2005.

[13] V.S. Chan, A.L. Heyes, D.I. Robinson, and J.T. Turner. Iodine absorption filters for Doppler global velocimetry. Measurement Science and Technology, 6(6):784–794, June 1995.

[14] R.W. Ainsworth, S.J. Thorpe, and R.J. Manners. A new approach to flow-field measurement — a view of Doppler global velocimetry techniques. International Journal of Heat and Fluid Flow, 18(1):116–130, February 1997.

[15] B. Leporcq, J.F. Le Roy, B. Pinchemel, and C. Dufour. Interest of a CW dye laser in Doppler Global Velocimetry. In ASME 1996 Fluids Engineering Division Conference, volume 4, 1996. FED-Vol. 239.

[16] G.S. Elliott and T.J. Beutner. Molecular filter based planar Doppler velocimetry. Progress in Aerospace Sciences, 35(8):799–845, November 1999.

[17] Y. Yeh and H.Z. Cummins. Localized fluid flow measurements with an He-Ne laser spectrometer. Applied Physics Letters, 4(10):176–178, May 1964.

[18] G.E. Devlin, J.L. Davis, L. Chase, and S. Geschwind. Absorption of unshifted scattered light by a molecular I_2 filter in Brillouin and Raman scattering. Applied Physics Letters, 19(5):138–141, September 1971.

[19] H. Shimizu, S.A. Lee, and C.Y. She. High spectral resolution lidar system with atomic blocking filters for measuring atmospheric parameters. Applied Optics, 22(9):1373–1381, May 1983.

[20] J. Tellinghuisen. Resolution of the visible-infrared absorption spectrum of I_2 into three contributing transitions. The Journal of Chemical Physics, 58(7):2821–2834, April 1973.

[21] S. Gerstenkorn and P. Luc. Atlas du spectre d'absorption de la molécule d'iode 14800 ¡ 20000 cm¡1. Éditions du Centre National de la Recherche Scientifique, 1978.

[22] J.N. Forkey, W.R. Lempert, and R.B. Miles. Corrected and calibrated I_2 absorption model at frequency-doubled nd:yag laser wavelengths. Applied Optics, 36(27):6729–6738, May 1997.

[23] M. Samimy and P. Wernert. Review of planar multiplecomponent velocimetry in high-speed flows. AIAA Journal, 38(4):553–574, April 2000.

[24] T.J. Quinn and J.-M. Chartier. A new type of iodine cell for stabilized lasers. IEEE Transactions on Instrumentation and Measurement, 42(2):405–406, April 1993.

[25] J. Crafton, C.D. Carter, and G.S. Elliott. Threecomponent phase-averaged velocity measurements of an optically perturbed supersonic jet using multicomponent planar Doppler velocimetry. Measurement Science and Technology, 12(4):409–419, April 2001.

[26] H. Buchet. Contribution au développement d'un vélocimétre à effet Doppler en vue de l'application aux turbomachines. Thèse de Doctorat spécialité Thermique et énergétique, École Centrale de Lyon, Ecully, France, March 2002. N± d'ordre 2002-09.

[27] J.N. Forkey, N.D. Finkelstein, W.R. Lempert, and R.B. Miles. Demonstration and characterization of filtered Rayleigh scattering for planar velocity measurements. AIAA Journal, 34(3):442–448, March 1996.

[28] Ph. Barricau, Ch. Lempereur, J.M. Mathé, H. Buchet, and A. Mignosi. Mise en oeuvre d'un dispositif innovant d'étalonnage temps réel pour la technique DGV (Doppler Global Velocimetry). In 8ème Congrès Francophone de Vélocimétrie Laser, Orsay, France, September 17–20, 2002.

[29] J. Salvi, X. Armangué, and J. Batlle. A comparative review of camera calibrating methods with accuracy evaluation. Pattern Recognition, 35(7):1617–1635, July 2002.

[30] C.E. Willert. Assessment of camera models for use in planar velocimetry calibration. Experiments in Fluids, 41:135–143, 2006.

[31] H. Zollner and R. Sablatnig. Comparision of methods for geometric camera calibration using planar calibration targets. InW. Burger and J. Scharinger, editors, Digital Imaging in Media and Education, Proc. of the 28th Workshop of the Austrian Association for Pattern Recognition (OAGM/AAPR), volume 179, pages 237–244, Hagenberg, Austria, 2004. Schriftenreihe der OCG.

[32] G. Toscani. Système de calibration et perception du mouvement en vision artificielle. PhD thesis, Université de Paris-sud, 1987.

[33] M. Bénallal. Système de calibration de caméra, localisation de forme polyèdrique par vision monoculaire. Mathématiques appliquées, École des Mines de Paris, November 2002.